EURASIAN JOURNAL OF MATHEMATICAL AND COMPUTER APPLICATIONS
ISSN 2306–6172
Volume 12, Issue 3 (2024) 61 – 72

PHYSICAL AND NUMERICAL SIMULATION OF HEAT AND MASS TRANSFER IN THE FURNACE OF A THERMOGRAVIMETRIC ANALYZER

Maslennikov G. E., Nikitina G. I., Nikitin A. D., Osipov P. V., Ryzhkov A. F.

Abstract A numerical study of the processes of heat and mass transfer in the furnace of a thermogravimetric analyzer was carried out, aimed at improving the accuracy of determining the kinetic characteristics of samples during their thermal transformations in different media. Validation of the model and prognostic estimates were carried out in relation to specially conducted thermogravimetric studies of the conversion of fossil and renewable carbon-containing raw materials in successive processes of decarbonization (combustion) and carbonation (mineralization of ash residue). The application of the study results allows to calculate the actual concentrations of the reagent over the sample uncontrolled by the device during pulsed switching of media and the actual temperatures of the sample during its thermochemical transformations.

Key words: numerical simulation, thermogravimetric experiment, concentration and temperature error, Peclet number, Arrhenius equation.

AMS Mathematics Subject Classification: 80A30.

DOI: 10.32523/2306-6172-2024-12-3-61-72

1 Introduction

Modern researchers [1, 2] widely use the practice of numerical simulation when conducting thermoanalytical studies of the behavior of chemically reacting systems using thermogravimetric analysis (TGA). It allows obtaining more accurate information related to the parameters that determine the thermochemical situation in the area of the sample under study, since standard controls provide indirect information corresponding to measuring points remote from the sample. As a result, a marked temperature and concentration unbalance may appear, forming a quite significant systematic concentration and temperature error, leveling the results of fine studies of the kinetics of heterogeneous processes, identifying the catalytic effects of impurities and additives.

The concentration unbalance will be most marked in the transient modes that occur during the pulsed switching of gas flows, and is associated, along with the transport delay τ_1, with the diffusive blurring of the reagent front, which occurs during the time τ_2.The ratio between convective (molar) and diffusive (molecular) transport is characterized by the Peclet number (Pe_d) [3, 4]:

$$Pe_d = \frac{wL}{D},$$

where w is the gas velocity, m/s; L is the characteristic size (TGA furnace height); D is the diffusion coefficient, m^2/s.

The Pe_d varies between $\sim$ 3–5 to $\sim$ 50–90 within the operating range of flow rates and temperatures for a number of media used in TGA, to our estimates (Fig. 1), which will form different dynamics of filling the furnace with reagent. The calculation uses the diffusion coefficient for a binary gas-nitrogen mixture calculated using the Lennard-Jones potential to the data [5]. Processing thermogravimetry data not including the actual concentration of the reagent will distort the course of the Arrhenius curve and shift the value of the pre-exponential coefficient.

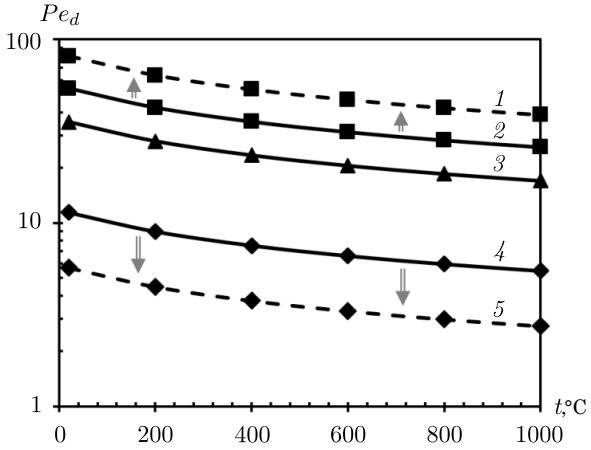

Figure 1: Calculation of Pe_d for different gases: *1* — CO_2 (12 nl/h), *2* — CO_2 (8 nl/h), *3* — H_2O (8 nl/h), *4* — H_2 (8 nl/h), *5* — H_2 (4 nl/h).

The temperature unbalance is most marked when chemical reactions with a non-zero thermal effect occur in the sample. For example, the overheating of the lower surface of the crucible holder with a bed of combusted coal particles compared to an empty crucible in study [6] $\sim$ 50°C. At the same time, the temperature difference between the sample and the lower surface of the holder is not controlled, which negatively affects the accuracy of determining the thermal effect of the reaction and the response rate constant. The reaction rate constant as a function of temperature $k(T)$ can be expressed only in terms of the activation energy E_a, knowing the coordinates of the poles k^* and T^* [7] by the formula:

$$k(T) = k^* \exp\left[-\frac{E_a}{RT}\left(1 - \frac{T}{T^*}\right)\right].$$

If the temperature error is relatively small ($\Delta T < 20$°C), then the error in determining the activation energy is as follows:

$$\frac{\Delta E_a}{E_a} \approx \frac{\Delta T}{T}.$$

Example [6]: failure to take into account the sample body overheating relative to the bottom and the thermal resistance of the bottom may set the determining temperature

too low by $\Delta\, T \approx 10°\mathrm{C}$, which reduces the value of the activation energy $\Delta E_a/E_a$ by 1.1%.

The paper aims at numerical simulation and test validation of heat and mass transfer in the characteristic modes of the TGA furnace, designed for fine processing of experimental results.

2 Testing

2.1 Materials

The study used five materials placed on a thermogravimetric holder in a crucible with an inner diameter of 5 mm and a depth of 4 mm:

- (K) calcium oxide powder (CaO $> 98\%$ by weight);
- ($A1$) monolithic particle anthracite (ash content 11%, moisture content 2% , volatiles 7%) in the form of a cylindrical tablet with a diameter of 5 mm and a height of 2 mm;
- ($A2$) crushed anthracite of 90-200 μm;
- ($D1$) monolithic particle of charcoal (ash content 3%, moisture content 2%, volatiles 17%) in the form of a cylindrical tablet with a diameter of 5 mm and a height of 2 mm
- ($D2$) crushed charcoal of 90-200 μm.

2.2 Test units

The tests were carried using NETZSCH STA 449 F3 thermogravimetric analysis device combined with QMS 403C Aëolos quadrupole mass spectrometer Fig. 2a. The TGA device consists of a thermostatically controlled unit of high-precision scales and a lifting furnace with an electric heater, allowing tests to be carried out in the temperature range up to 1250 °C. According to the passport data, the relative error of mass measurement does not exceed $\pm 0,1\%$, temperature $\pm 0,5\%$.

To protect the weighing unit from gases in the furnace, argon is supplied to the furnace through it with a flow rate of 60 ml/min, the flow rate is controlled by a mass flow regulator. The working gas is supplied to the furnace from a cylinder, the gas flow is regulated by a needle valve and measured with a rotameter. The gas enters the lower part of the furnace, warms up during lifting in an annular channel along the furnace wall, and goes from top to bottom, flowing around the holder with a sample(Fig. 2b). At the outlet of the furnace, a sample of gases is taken for analysis in a mass spectrometer, the remaining gases go to the exhaust system. The method of gas analysis using a mass spectrometer is described in [8].

A sample of the test material is placed on a holder and continuously weighed when testing. The temperature measurement is performed using T_1 thermocouple, which is part of the holder and is located under the sample. To obtain a signal of differential

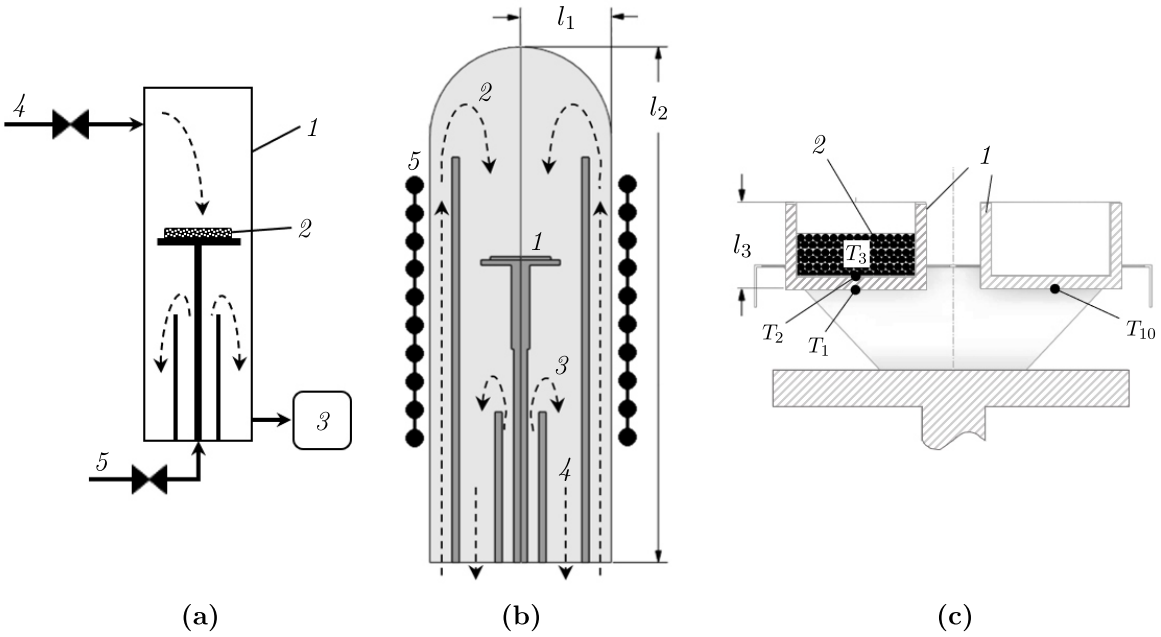

(a) **(b)** **(c)**

Figure 2: Test unit scheme (a): *1* is TGA furnace, *2* is sample, *3* is mass spectrometer, *4* is working gas supply, *5* is protective gas supply; TGA furnace geometry (b): *1* is sample, *2* is working gas, *3* is protective gas, *4* is gas outlet, *5* is heater; DSC holder geometry (c): *1* is crucibles, *2* is sample.

scanning calorimetry (DSC), which characterizes the thermal effect of a chemical reaction, a holder with two thermocouples is used (Fig. 2b), one of which signal T_1 is located under a crucible with a sample, the second T_{10} is a control thermocouple under an empty (reference) crucible. The following temperature designations are used in the study:

T_1 is the crucible (with sample) outside temperature;

T_2 is the crucible (with sample) inside temperature;

T_3 is the average temperature of the sample in the crucible;

T_{10} is the empty (reference) crucible temperature;

$\Delta T_{3-1} = (\Delta T_{3-2} + \Delta T_{2-1}) = ((T_3 - T_2) + (T_2 - T_1))$ is overheating of the sample in relation to the signal thermocouple T_1;

$\Delta T_{1-10} = (T_1 - T_{10})$ is overheating of the signal thermocouple in relation to the test thermocouple;

$\Delta T = (\Delta T_{3-1} + \Delta T_{1-10})$ is the overall error of the DSC method in determining the sample temperature.

2.3 Test procedure

The test procedure is shown in Table. 1. A baseline correction was additionally performed for experimental curves.

The flow rate of the working gas under normal conditions in all tests was 8 l/h.

Tests 1–2 were conducted to obtain data on the dynamics of filling the furnace space with a reagent gas with a pulse supply of CO_2 in two modes: at 30 °C (cold)

and 500 °C (hot). The type of sample holder is thermogravimetric (TG). Tests 3–6 were carried out to obtain data on the temperature difference $\Delta T = \Delta T_{1-10} = T_1 - T_{10}$ between thermocouples of empty and filled crucibles during the combustion of heating samples in the air. The type of sample holder is thermogravimetric with differential scanning calorimetry (TG-DSC).

Table 1: Tests procedure

№	Material	Holder type	Sample weight, mg	Temperature program	Working gas Composition, % vol.
1	Empty	TG	0	Stage one: holding at 30°C during 10 min Stage two: holding at 30°C during 5 min	Stage one: 100% N_2 Stage two: 77% N_2 + 23% CO_2
2	Calcium oxide (K)	TG	31.0	Stage one: heating from 20 to 500°C at the rate of 20°C/min Stage two: holding for 500°C during 20 min Stage three: holding at 500°C during 40 min	Stage one: 100% N_2 Stage two: 100% N_2 Stage three: 77% N_2 + 23% CO_2
3	Anthracite tablet ($A1$)	TG -DSC	54.1	Stage one: heating from 20 to 900°C at the rate of 25°C/min Stage two: holding for 900°C during 20 min Stage three: cooling to 400°C at the rate of 15°C/min Stage four: heating from 400 to 1000°C at the rate of 7.5°C/min	Stage one: 100% Ar Stage two: 100% Ar Stage three: 100% Ar Stage four: 100% air.
4	Anthracite powder ($A2$)	TG -DSC	52.0		
5	Charcoal tablet ($D1$)	TG -DSC	15.8		
6	Charcoal powder ($D2$)	TG -DSC	23.2		

3 TGA furnace numerical simulation of heat and mass transfer.

Two numerical models of TGA in the study, aimed at solving the following independent objectives: the filling dynamics calculation of the furnace space with a reagent gas during its pulsed supply (model I) and the temperature field calculation in the holder area by the combustion of the material under study (model II).

3.1 The furnace filling model description with a reagent gas (model I).

The analyzer furnace with a TG holder is axisymmetric, so the geometry is two-dimensional for half of the section of the internal space. The design area of the model includes an annular channel for supplying a mixture of gases, a sample holder with a

plate where a bed is set, an annular channel for supplying protective gas, an annular channel for exhaust gases (Fig. 2b). To perform the calculations, a fine grid consisting of 128262 quadrangular cells and 132217 points was taken.

The gas flow type in TG furnace is laminar. The motion of the gas medium is described by the Navier-Stokes equation and the continuity equation. The density of the supplied gases is calculated by the ideal gas equation. The gas includes components such as O_2, N_2, H_2O, and CO_2. The local mass fractions of each Y_i substance are predicted by solving the convection-diffusion equation. This equation, in the absence of internal (chemical) sources of substances, has the following general form:

$$\frac{\partial}{\partial \tau}(\rho Y_i) + \nabla\left(\rho \vec{w} Y_i\right) = -\nabla \vec{J}_i,$$

where $\vec{J}_i$ is the diffusion flow arising from the concentration gradient, expressed by Fick's law, for which the diffusion coefficient is calculated using the Lennard-Jones potential [9]. This equation is solved for $N-1$ chemical components present in the system, where N is their total number in the gas phase.

The dependence of the heat capacity on the temperature of gaseous components, as well as corundum walls, is given through piecewise polynomial functions [10, 11]. The radiation is solved by the method of discrete ordinates with discretization of the radiation transfer equation by 5 divisions and 3 pixels [12]. The gas absorption coefficient is predicted by a weighted sum of gray gas models. The dependence of the wall emissivity on temperature is given by a polynomial dependence [13].

The calculation algorithm for filling the furnace with reagent gas is as follows: first, a stationary calculation is performed, corresponding to the conditions in the furnace before the supply of CO_2, when the main gas supplied is N_2;
then the resulting solution is used as an initial condition for dynamic calculation. At the same time, the composition and velocity of the main gas at the inlet change, and the parameters of the protective gas remain unchanged. The calculated flow time is 180 s, the time step is 0.1 s. Table 2 shows the boundary conditions of the completed calculations according to Model I.

3.2 Description of the temperature field model in the holder area (Model II)

Fig. 2b shows the geometry of model II with TG-DSC holder. Corundum crucibles are placed on a platinum plate. Temperature is measured at two points T_1 and T_{10}, the thermocouples are fixed under each crucible plate. The calculated area is made three-dimensional for half of the furnace (mirror-like). The tetrahedral grid contains 2072302 points and 586994 cells.

The hydrodynamic multiphase granular Euler model is used to implement a loose bed having nonzero porosity [14]. The parameters of the gas phase are identical to model I. Depending on the simulated experiment, the solid phase consists of particles of anthracite or charcoal with a diameter of 130 μm, the parameters of the studied samples are shown in Table 3 The thermal conductivity coefficient of the fuel particle

Table 2: Model I boundary conditions

Calculation type			Cold stationary	Cold non-stationary	Hot stationary	Hot non-stationary
Wall temperature, K	heater		303		881	
	top (dome)		303		773	
	non-heating side wall *		303		$68 \cdot \exp(0.0069 h_c)$	
Basic gas	volume composition, %	N_2	98.87	77.08	99.24	76.49
		CO_2	0.27	22.13	0.07	22.97
		O_2	0.69	0.62	0.53	0.41
		H_2O	0.17	0.17	0.16	0.13
	rate under normal conditions, m/s		0.00255	0.00292	0.00230	0.00264
	temperature, K		303		423	
Protective gas	volume composition, %	Ar	100		100	
	rate under normal conditions, m/s		0.016		0.016	
	temperature, K		303		373	

*hot mode: non-heating side wall temperature is set as an exponential function of the wall height (h_c, mm)

is calculated as follows [15]:

$$\lambda = \lambda_{true} \left(1 - \mathrm{P}^{2/3}\right),$$

where P is the fuel particle porosity, λ_{true} is the thermal conductivity coefficient of the fuel particle material.

The heat transfer between the solid and gaseous phases is calculated according to Gann's law [16]. In this study, the response submodel is not used, instead, the internal heat sources (heat released during fuel combustion) are set based on the current rest combustion rate $dm/d\tau$ and distributed in an area with a height of 0.1 mm over the entire sample section at a level inversely proportional to the current degree of conversion X.

Table 3: Samples characteristics for Model II

Parameter	Designation	Anthracite	Charcoal
Porosity	P	0.178	0.788
True density, kg/m^3	P_{true}	1900	1600
Apparent density, kg/m^3	$\rho_{apparent}$	1562	339
True thermal conductivity, W/m·K	λ_{true}	$0.512019 + 0.000702(\mathrm{T} - 273)$	1.02
Low heat level, MJ/kg	Q	30.60	32.64

The boundary conditions for the calculations performed according to Model II are shown in Table. 4. The supplied gas is air, its velocity at normal conditions is 4.06 mm/s and is the same for all tests.

Table 4: Model II boundary conditions for

Calculation #	1	2	3	4	5	6	7	8
Material	$A2$	$A2$	$A2$	$A2$	$A2$	$A1$	$D2$	$D1$
Bed depth h, mm	2.7	2.7	2.7	2.7	2.7	2.0	2.7	2.0
Bed porosity ε	0.50	0.50	0.50	0.50	0.50	0.0	0.44	0.0
Conversion rate X	0.05	0.1	0.5	0.9	0.99	0.5	0.5	0.5
Combustion rate, mcg/s	7.5	12.5	24.1	19.8	8.2	26.2	24.7	26.4
The furnace wall and the supplied gas temperature, K	764	781	863	949	1001	1005	788	805

4 Results.

4.1 Calculation results based on model I.

Acceleration profiles of CO_2 concentration over the bed and at the furnace outlet were obtained based on model I calculations. Figure 3 shows a comparison of the calculation results with the test data for cold and hot modes, in both cases there is a good coincidence of curves, which indicates the adequacy of the model.

When increasing temperature, the rate of CO_2 increase in concentration becomes higher. The stabilization time of CO_2 concentration for the cold mode is ~ 120 seconds, for the hot mode is 60 seconds

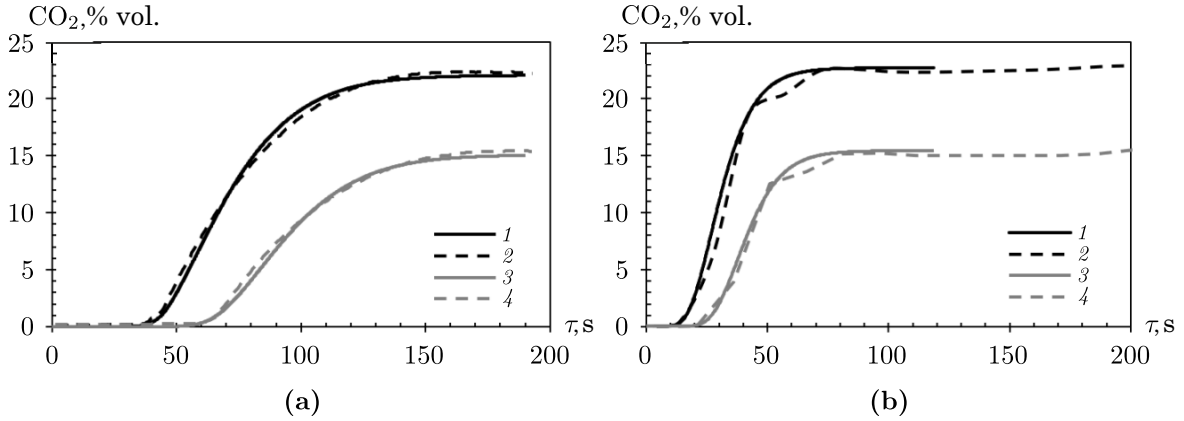

Figure 3: The model validation: cold mode (a), hot mode (b); *1* is numerical calculation (over bed), *2* is test (over bed), *3* is numerical calculation (furnace outlet), *4* is test (furnace outlet).

Figure 4 shows a comparison of cold and hot modes. For clarity, Figure 4b shows the dynamics in dimensionless coordinates, where the ratio of the current time τ to the characteristic convective transfer time $\tau_k = V_{\text{TGA}}/G$ is deposited on the abscissa axis, where V_{TGA} is the volume of the furnace TGA, G is the volume flow rate of the supplied gas. For the cold mode, $\tau_k = 62$ s, for the hot mode, $\tau_k = 24$. In this setting, when the variable value of the convective flow velocity is not considered, for the hot mode, a decrease in CO_2 growth due to diffusion blurring of the flow front becomes noticeable. The actual transfer time for the cold mode (30 °C) turns out to be ~ 2

times higher than the time of the convective transfer; for the hot mode, this difference increases to 3-4 times.

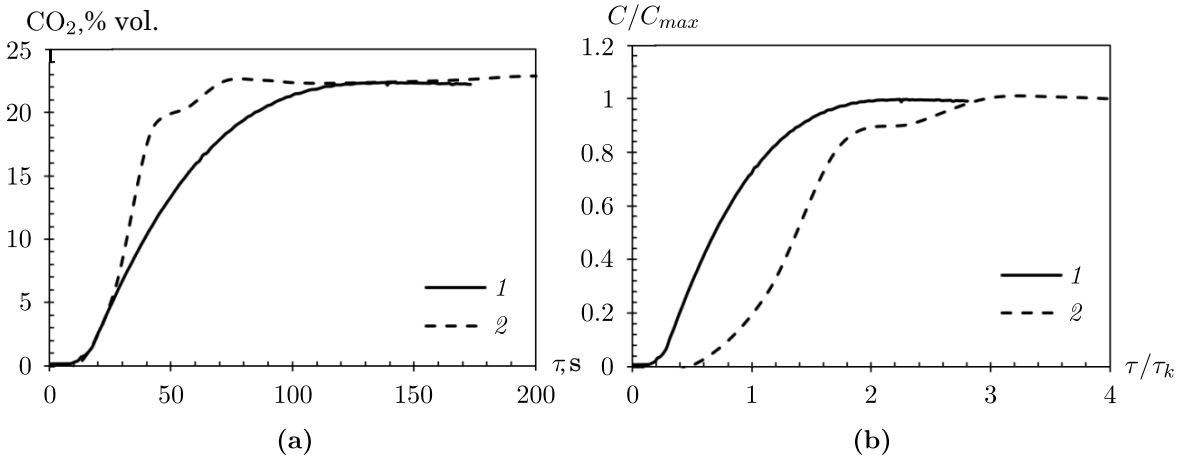

Figure 4: Comparison of the dynamics of CO_2 concentration growth in cold (1) and hot (2) modes in real (a) and nondimensional (b) coordinates.

4.2 Calculation results based on model II.

As a result of calculations based on model II, the temperature distribution in the holder area during the combustion of the studied material was obtained. The key points and their interpretation are given in Section 2.2. Validation was performed by the temperature difference ΔT_{1-10} during the combustion of anthracite dust. Fig. 5a shows a comparison of the results of numerical calculation with the test data and analytical calculation from [6]. Figure 5b shows the obtained temperature differences ΔT_{2-1}, ΔT_{3-2} and ΔT_{3-1}.

At the beginning of the reaction, when heat emissions are concentrated in the upper part of the sample, the deviation of the sample average temperature from the readings of the T_1 thermocouple is the largest and is 15 °C, this is due to the fact that as the combustion progresses, this difference decreases and, when only the sample bottom combusts, it can become negative, however, this moment shall be clarified, since the model does not consider a change in the sample volume.

Table 5 shows the key temperature deviations obtained as a result of simulation for four samples at the time of conversion degree $X = 0.5$.

Table 5: Temperature deviations during the combustion of half the mass of samples of various nature

ΔT[°C]	$A1$	$A2$	$D1$	$D2$
ΔT_{1-10}*	41/44	39/40	43/43	52/52
ΔT_{2-1}	1	1	2	2
ΔT_{3-1}	5	10	47	54

*numerator is calculation, denominator is test

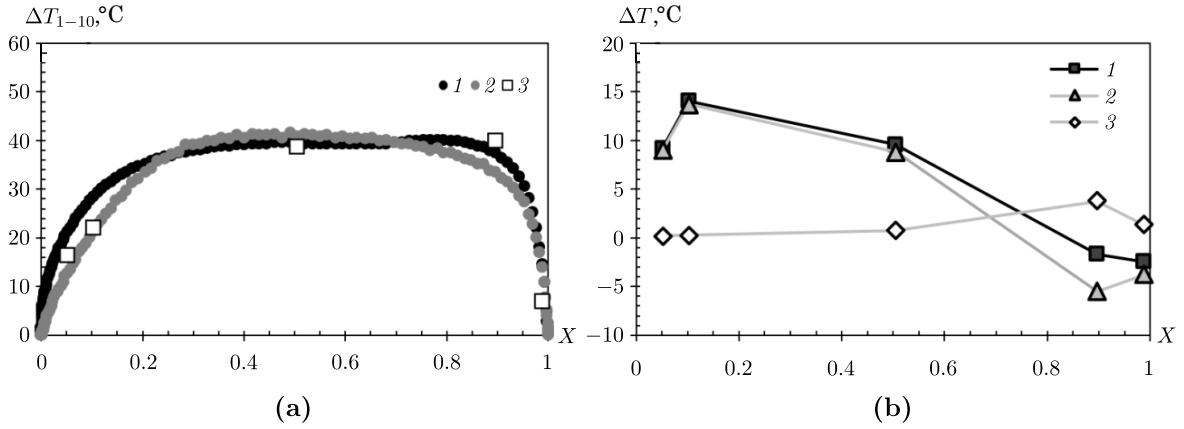

Figure 5: Temperature deviations during the combustion of anthracite $A2$ dust: (a) validation by the DSC ΔT_{1-10} *1* is test data, *2* is analytical calculation [6], *3* is numerical simulation; (b) calculation of other temperature deviations *1* is ΔT_{3-1}, *2* is ΔT_{3-2}, *3* is ΔT_{2-1}.

Figure 6 shows the temperature distribution through the crucible height and bed depth for the samples under study at the time of the degree of conversion $X = 0.5$. Depending on the properties of the materials, ΔT_{3-1} difference varies significantly.

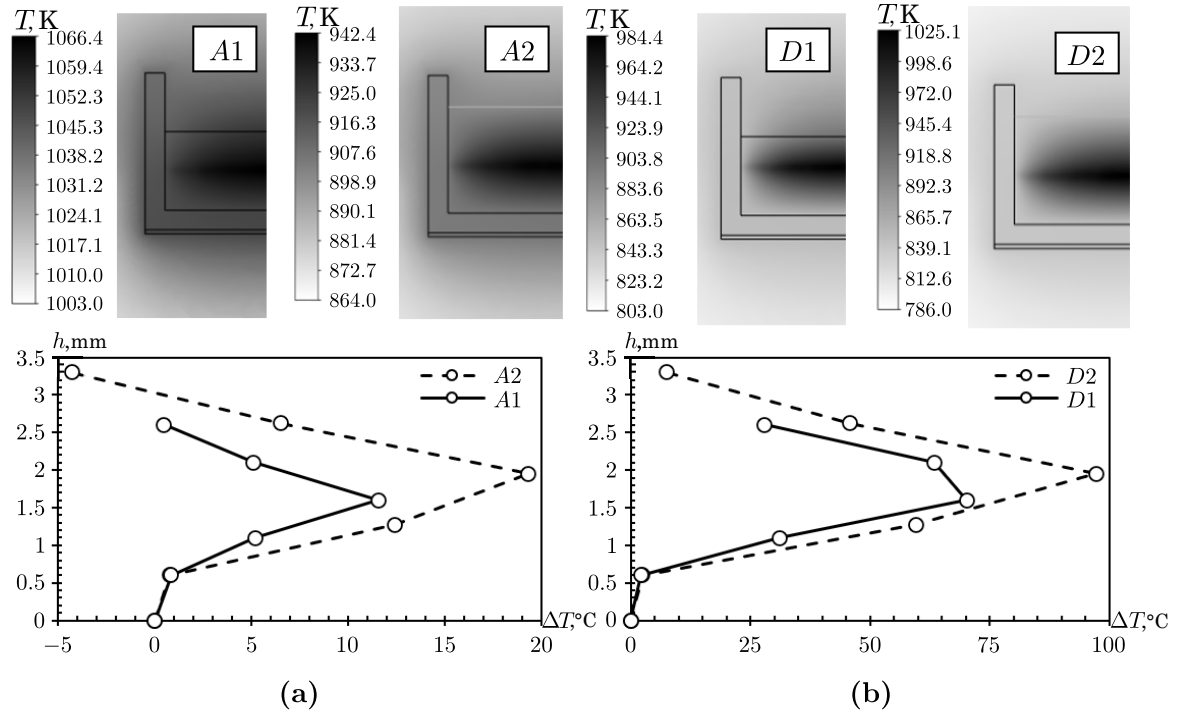

Figure 6: Visualization of the temperature field and temperature distribution through the crucible height and bed depth for anthracite (a), charcoal (b) at $X = 0.5$ to numerical simulation data.

The highest value was obtained for charcoal, which has high porosity and, accordingly, low thermal conductivity. For it, the error in determining the average temperature of

the sample using a thermocouple is 5–10 times higher than for anthracite and reaches 50-60 °C, which may underestimate the activation energy determined in the test by $\Delta_a/E_a = 6-7\%$. In this case, the local temperature value in the heat release region can be 100 °C higher than that determined by thermocouple, as shown in Fig. 6.

5 Conclusion

The study performed using numerical simulation and physical thermogravimetric experiment revealed the presence of a significant concentration and temperature error due to the development of complex heat and mass transfer processes uncontrolled by the standard means of the device, which are most significantly occur when pulsed switching of gaseous media and during intense heat release in the studied sample. The uncontrolled concentration of the reagent near the sample during pulsed switching of gaseous media increases near the sample not instantly, but over a period of time determined by the competition of molar (convective) and molecular (diffusion) transport. The transition time for the heaviest gas (CO_2) in the working range is 2-4 times longer than the convective transfer time, which requires appropriate correction of TGA test processing program. The greatest local overheating of the samples, uncontrolled by the device, was obtained during the exothermic oxidation process of charcoal and amounted to 100 °C or 11.5% of the controlled level of the thermocouple in the furnace space. Considering overheating increases the accuracy of determining the activation energy of the reaction by 6–7%.

Acknowledgement

The research funding from the Ministry of Science and Higher Education of the Russian Federation (Ural Federal University Program of Development within the Priority-2030 Program) is gratefully acknowledged.

References

[1] Baath Y.S., Nikrityuk P.A., Gupta R., *Experimental and numerical verifications of biochar gasification kinetics using TGA*, Renewable Energy, Vol. 185, (2022), P. 717-733.

[2] An F., Kuster F., Ackermann R., Guhl S., Richter A., *Heat and mass transfer analysis of a high-pressure TGA with defined gas flow for single-particle studies*, Chemical Engineering Journal, Vol. 411, (2021), 128503.

[3] Gukhman A. A. *Introduction to Similarity Theory*, M.: Vyshchaya Shkola, 1963.

[4] Kutaladze S. S. *Fundamentals of the theory of heat transfer*, Novosibirsk: Nauka, 1970.

[5] Sherwood Pў., Pigford R., Willkie C. *Mass Transfer* [Russian translation], M.: Khimiya, 1982.

[6] Khudiakova, G. I., Amarskaya I. B., Belousov V. S. *The influence of fuel particle bed depth in the thermogravimetric investigation of coal conversion*, Sb. materialov dokl. IX mezhdunar. seminara vuzov po teplofizike i energetike, Vol. 1, (2015), P. 122-131.

[7] Pomerantsev V. V. *Fundamentals of Practical Combustion*, Leningrad: Energoatomizdat, 1986.

[8] Nikitin A. D., Nyashina G. S., Ryzhkov A. F., Strizhak P. A. *Anthropogenic emissions from the combustion of composite coal-based fuels*, Science of The Total Environment, Vol. 772, Article 144909 (2021).

[9] McGee H. A. *Molecular Engineering*, N. Y.: McGraw-Hill, 1991.

[10] McBride B. J., Gordon S, Reno M. A., *Coefficients for Calculating Thermodynamic and Transport Properties of Individual Species*, NASA TM-4513, 1993.

[11] *Aluminium oxide (Al2O3)*, http://qedfusion.org/LIB/PROPS/PANOS/al2o3.html.

[12] Chui E. H., Raithby G. D. *Computation of radiant heat transfer on a nonorthogonal mesh using the finite-volume method*, Numer. Heat Tr. B Fund., Vol. 23., N 3. (1993), P. 269–288.

[13] Hampartsoumian E., Hainsworth D., Taylor J. M., Williams A., *The radiant emissivity of some materials at high temperatures — Review*, J. Energy Inst., Vol. 74, (2001), P. 91–99.

[14] Chiesa M., Mathiesen V., Melheim J. A., Halvorsen B., *Numerical Simulation of Particulate Flow by the Eulerian—Lagrangian and Eulerian-Eulerian Approach with Application to a Fluidized Bed*, Comput. Chem. Eng., Vol. 29., N 2. (2005), P. 291–304.

[15] Misnar A. *Thermal conductivity of solids, liquids, gases and their compositions*, M.: Mir, 1968.

[16] Gunn D. J. *Transfer of Heat or Mass to Particles in Fixed and Fluidized Beds*, Int. J. Heat Mass Transf., Vol. 21., N. 4. (1978), P. 467–476.

Maslennikov G.E.,
Ural Federal University,
19 Mira Str., 620002 Yekaterinburg, Russia
Email: g.e.maslennikov@urfu.ru,

Nikitina G.I.,
Ural Federal University,
19 Mira Str., 620002 Yekaterinburg, Russia
Email: uge87@mail.ru,

Nikitin A.D.,
Ural Federal University,
19 Mira Str., 620002 Yekaterinburg, Russia
Email: nikitin.alexander@urfu.ru,

Osipov P.V.,
Ural Federal University,
19 Mira Str., 620002 Yekaterinburg, Russia
Email: p.v.osipov@urfu.ru,

Ryzhkov A.F.,
Ural Federal University,
19 Mira Str., 620002 Yekaterinburg, Russia
Email: a.f.ryzhkov@urfu.ru.

Received 06.04.2024, Accepted 28.06.2024